ALOS-2 InSAR Component for SCEC Community Geodetic Model

Report for SCEC Award # 19042
Submitted March, 31, 2020

Investigators: Roland Bürgmann (UCB), Paul Lundgren (JPL), Eric Fielding (JPL), Zhen Liu (JPL), Kang Wang (UCB)

Introduction

One major task of SCEC5 is to develop a Community Geodetic Model (CGM) for use by the SCEC community in system-level analyses of earthquake processes over the full range of spatial and temporal scales. The CGM is built on the complementary strengths of temporally dense GPS data and spatially dense InSAR data. For the InSAR part, much of the community effort has focused on the C-band Sentinel-1 data, which are featured by regular and dense acquisitions (12 days) over the entire SCEC region. The C-band Sentinel-1 SAR data, however, sometimes suffer from phase decorrelation in mountainous and vegetated areas. For example, in the Coachella Valley just south of the Salton Sea, phase decorrelation due to the widespread farming makes the ground movement measurement with C-band interferometry less straightforward, even though this region is experiencing fast ground deformation as a result of active and intense geothermal production and tectonic deformation along the Brawley seismic zone and Imperial Fault. L-band SAR data, on the other hand, can maintain a relatively high radar coherence over vegetated areas. This project is aimed at contributing to the CGM by providing L-band ALOS-2 derived secular velocities and time series products for southern California. This effort includes data processing, error analysis and mitigation, and development of velocity and time series products suitable for integration with GNSS and other InSAR datasets for the CGM. This effort complements SCEC projects by Sandwell and Liu, and Fialko and Tymofyeyeva who are focused on C-band Sentinel-1 InSAR analysis. The methods and computer codes developed in this study are also useful for mitigating the temporally or spatially correlated noise in InSAR measurement of data from other missions, such as Sentinel-1 and NISAR.

Data processing

ALOS-2 data processing in this project is largely based on the work presented in Liang et al. (2018), updated with additional data acquired in the last two years. We use a full-aperture based processing workflow based on the JPL InSAR Scientific Computing Environment (ISCE) (Rosen et al., 2012) to process the ALOS-2 ScanSAR data to generate interferograms. Technical details about the approach can be found in Liang and Fielding (2017a). Here we briefly summarize the essential steps involved: 1) estimate the parameters (e.g., burst length, burst cycle length, raw burst start times etc.); 2) perform range bandpass filtering to extract common range spectrum; 3) resample the slave image if needed; 4) calculate burst overlap between master and slave images; 5) perform azimuth bandpass filtering to remove non-overlap spectra caused by Doppler centroid frequency difference and burst misalignment; 6) co-register the master/slave pair through cross-correlation; 7) form and mosaic subswath interferograms to generate each single-frame interferogram; 8) mosaic interferograms of multiple frames along-track to get the final

interferogram and do phase unwrapping. For ALOS-2 ScanSAR interferometry, ionosphere phase delay is a dominant noise source that needs to be properly corrected. We apply a range split-spectrum method that exploits the dispersive nature of the ionosphere (Gomba et al., 2016; Liang and Fielding, 2017b; Liang et al., 2018). The approach involves the generation of interferograms using two range subbands. The phases derived from subband interferograms are then combined to solve for dispersive (ionosphere) and non-dispersive phase components (e.g. surface deformation). For the track D165, 24 scenes were acquired from early 2015 to 2019, with which we generated 70 interferograms with high radar coherence and robust corrections for the ionospheric noises. Figure 1 shows the orbital baseline vs. time of the image acquisitions, as well as the interferograms that were used in the later velocity and time series analysis.

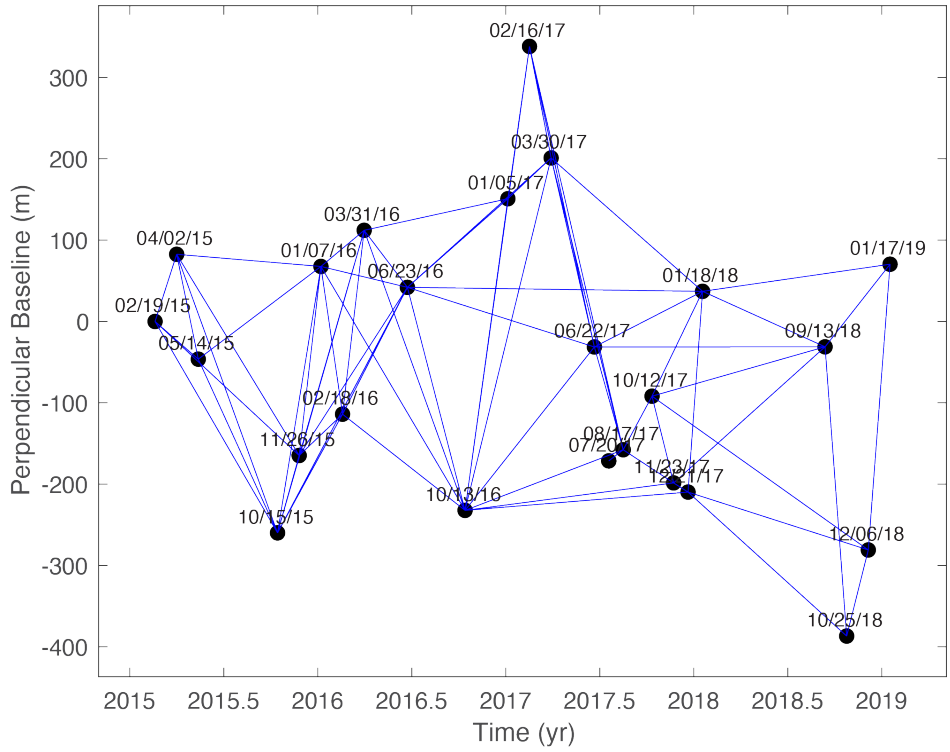

Figure 1. Baseline vs. time of ALOS-2 acquisitions along the descending track D165 over the study area. Black dots represent the SAR image acquisitions and blue lines represent the interferograms.

Corrections for atmospheric noise and time series analysis

The most significant limitations to InSAR measurements of a low-amplitude deformation, such as the interseismic deformation, arise from the variability of the ionosphere and variability of water vapor in the troposphere. We applied the SAR range split-spectrum corrections for the ionospheric effects as described above and in Liang et al. (2018). Here we discuss the tropospheric effects. One commonly used method for dealing with tropospheric noise is to stack many interferograms with different acquisition times, assuming that the tropospheric noise is random in time. This method is effective and easy to implement, but comes at the sacrifice of temporal resolution. In this project, we explored different methods to correct for tropospheric noise, including the ECMWF Re-analysis version 5 (ERA-5) weather model, and Common-Scene-Stacking (CSS) (Tymofyeyeva & Fialko, 2015).

We first correct for the large-scale tropospheric noise using the ERA-5 weather model. The ERA-5 weather model provides hourly estimates of a series of atmospheric variables, including temperature, pressure, specific humidity, geopotential at different height levels with a spatial resolution of ~30 km. These parameters can be then used to compute the tropospheric delay of the radar phase (e.g. Jolivet et al., 2011). Our implementation of the ERA-5 weather model correction is based on the TRAIN software (Bekaert et al., 2015). Figure 2 shows a comparison of LOS displacements between the ALOS-2 observations and ERA-5 model predictions for 30 interferograms (70 total) considered in this study. For most interferograms, both the spatial pattern and amplitude of range change predicted by the ERA-5 weather model are very similar to the ALOS-2 interferograms after ionospheric corrections, indicating that the large variations in range change across those interferograms are indeed mostly due to the tropospheric delays. Nevertheless, large residuals are still seen in some interferograms, which could be attributed to the relatively low spatial and temporal resolution of the current ERA-5 weather model. We anticipate that the performance of such corrections will continue to improve with future improvements of the weather model.

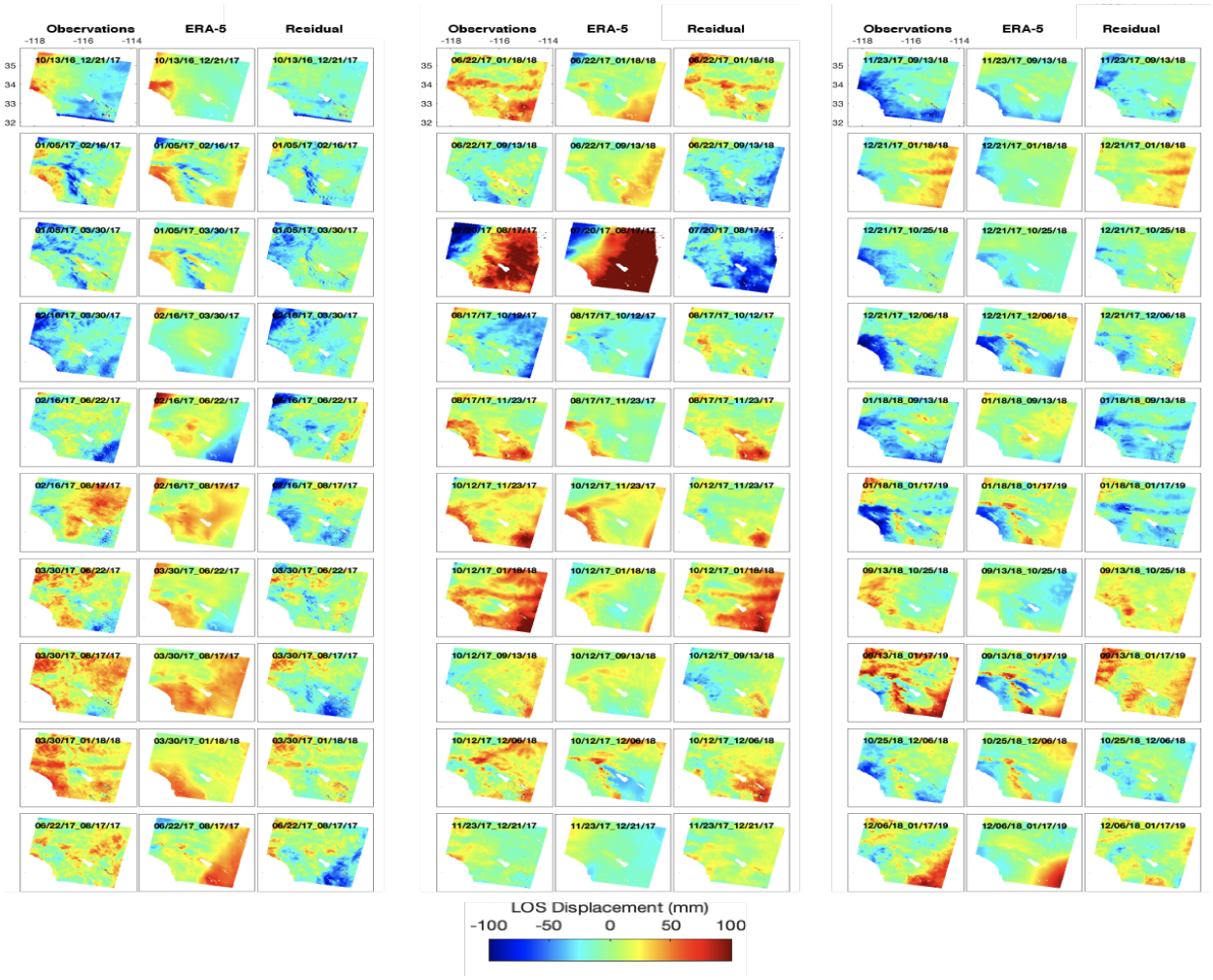

Figure 2. Comparison of range change between ALOS-2 observations and the ERA-5 weather model predictions for randomly selected 30 interferograms after the ionospheric noise correction along the descending T165.

We then apply the CSS (Tymofyeyeva & Fialko, 2015) to further suppress the high-frequency component of the atmospheric delay that is less coherent in time. This method takes advantage of the fact that interferograms sharing a common scene necessarily contain the same contributions from delays in the radar phase due to propagation effects (i.e. atmospheric delays). Stacking these interferograms will enhance the noise from that common scene, while reducing that from the rest, provided that the atmospheric noise contributions are random in time. It is therefore possible to estimate the atmospheric phase delay on a given scene, by stacking the interferograms that share a common scene, if tectonic deformation cancels out or can be estimated and removed during the stacking. We find this method is quite efficient in reducing the atmospheric noise with relatively regular and dense acquisitions, such as the Sentinel-1 data. For ALOS-2, the image acquisitions are not very frequent and regular in time (see Figure 1 for the image acquisition times), which limits the number of interferograms to stack for a given scene. To ensure the tectonic deformation 'cancels out' in the stacking process to estimate the atmospheric phase screen (APS), we further limit the stacking to only the symmetric interferograms; that is, the interferograms have symmetrical temporal spans on each side of the scene. This leads to only a limited number of scenes with APS estimates. Nonetheless, given that CSS is part of our standard processing chain, we still apply CSS to the ALOS-2 analysis in this study, although its performance in reducing the atmospheric noise may be limited compared to improvements from applying the ERA-5 weather model.

Velocity and time series

After correcting for noise due to the ionospheric and tropospheric perturbations, we derive the average line-of-sight (LOS) velocity and displacement time series using the Small Baseline Subset (SBAS) method (e.g. Berardino et al., 2002; Schmidt and Bürgmann, 2003). In contrast to previous studies utilizing ALOS-1 data (Tong et al., 2013), GPS data were not used to constrain the long-wavelength deformation field. Figure 3 shows the average LOS velocities derived from data of the descending track T165 and its comparison with the GPS measurements (Blewitt et al., 2018). The ALOS-2 LOS velocity field is characterized by a gradual increase of range change from northeast to southwest, consistent with the deformation pattern one would expect from the relative plate motion between the Pacific and North America plates. We compare the InSAR and GPS velocities projected on the SAR LOS along a profile A-A' that spans the San Andreas fault system and the East California Shear Zone. Figure 3b and c show the InSAR LOS velocities based on interferograms without and with atmospheric noise corrections, respectively. Although both results show a gradual increase in range-change rate from southwest to northeast, and roughly match the GPS velocities, the InSAR velocity profile without atmospheric noise correction exhibits strong oscillations between -50 to 50 km, and significantly deviates from the GPS observations (Figure 3b), which is likely attributable to the topographically corrected atmospheric delay in this area. We also compare the InSAR velocity solution derived in this study with the velocity solution of Liang et al. (2018), which used temporal smoothing to suppress atmospheric noise instead of external information (e.g, weather model and/or CSS based correction). In general, the same profile from both velocity solutions shows very similar agreement with *in-situ* GPS measurements. Further comparison would help identify optimal ways to integrate the two for CGM and quantify associated uncertainties.

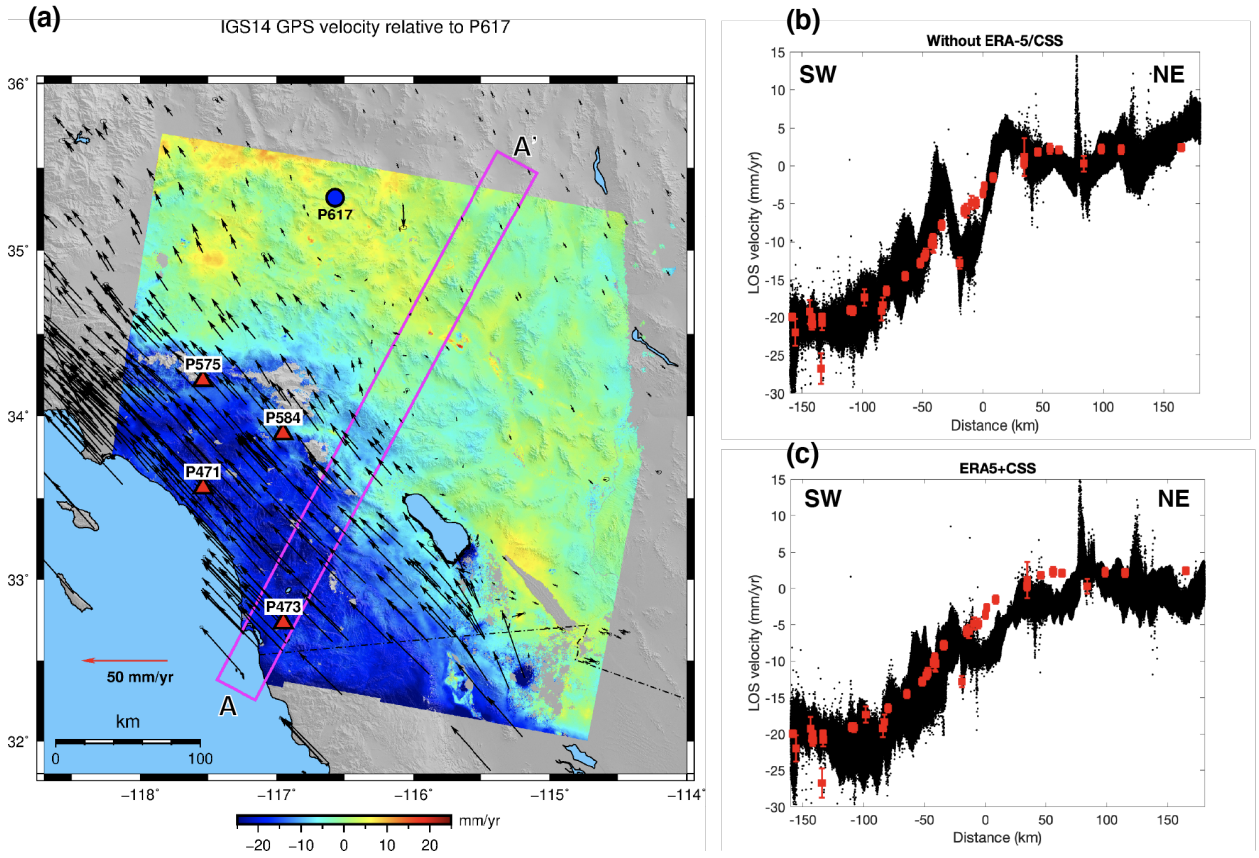

Figure 3. Comparison of average velocity between GPS and ALOS-2 observations. (a) color represents the ALOS-2 LOS velocity derived from SBAS analysis after ionospheric and tropospheric noise correction. Negative values correspond to ground motion away from the satellite. Black vectors are GPS velocities in the IGS14 reference frame, with the site P617 pinned to zero. (b) and (c) show the LOS velocities along a profile A-A' shown in (a) before and after corrections for the atmospheric noises, respectively. Note that the velocity profile without atmospheric noise correction exhibits strong oscillations from -50 to 50 km distance, and significantly deviates from the GPS observations (red circles). The GPS data were not used in deriving the InSAR velocity field.

Figure 4 shows the comparison of LOS displacement time series between GPS and ALOS-2 at a few GPS sites in the InSAR scene. Similar to the average velocity, we compare the solutions with and without atmospheric noise corrections as described above. It is clear that at all four GPS stations examined here, the time series with atmospheric corrections exhibit less scattering and match the GPS data more closely. In particular, we note that the scattering of the time series without atmospheric noise correction is as high as > 10 cm, whereas the solution with atmospheric noise correction exhibits much more modest deviations (< 5 cm) from the GPS time series. No temporal smoothing or function fitting is applied in our time series analysis. The temporal scattering would be further reduced if temporal smoothing is applied.

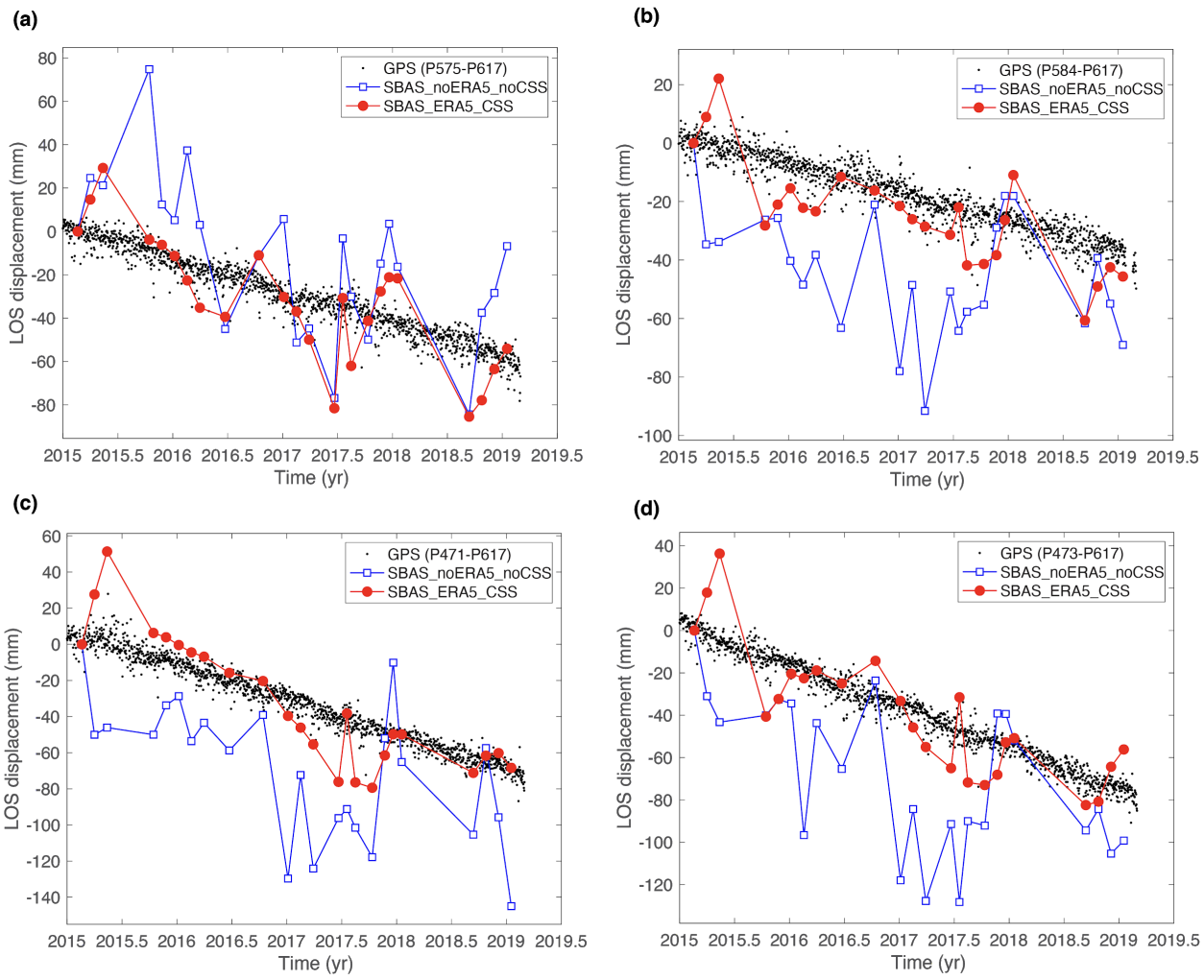

Figure 4. Comparison of LOS displacement time series between GPS and ALOS-2 observations at a few PBO GPS sites (shown as magenta triangles in Figure 3a). Black dots are the 3-D GPS displacement time series projected onto the line-of-sight of the ALOS-2 observation. Blue squares represent the ALOS-2 LOS displacement time series without correcting for the atmospheric noise. Red dots show the ALOS-2 time series after correcting for the atmospheric noise with the ERA-5 weather model and Common-Scene-Stacking. Note that no temporal smoothing was applied in the SBAS time series analysis.

In summary, ALOS-2 data are promising datasets complementing other InSAR data over southern California to build a comprehensive and reliable CGM. Specifically, as shown in Figures 3 and 4, both the average LOS velocity and displacement time series derived from data along the descending track T165 after ionospheric and tropospheric corrections are in good agreement with GPS measurements, even though no GPS data were used in our InSAR analysis. The data products derived with this project will also be compared with other InSAR datasets, such as Sentinel-1. We are currently working with other groups participating in the SCEC CGM project on how to integrate the data from different platforms and present the CGM in an accessible and unified format.

Acknowledgements

The ALOS-2 data used in this study was provided by the Japan Aerospace Exploration Agency (JAXA) under ALOS PI project (PI#3273). Original data is copyright 2015-2019 JAXA. Part of this research was performed at Jet Propulsion Laboratory, California Institute of Technology under contract with National Aeronautics and Space Administration and supported by the Earth Surface and Interior Focus Area.

Data and Software availability

The JAXA data license permits data sharing with Co-Investigators of the ALOS PI projects. The ALOS-2 InSAR processing was performed with the JPL InSAR Scientific Computing Environment (ISCE) version 2, which is available as open-source software on GitHub https://github.com/isce-framework/isce2. The ALOS-2 application in ISCE is "alos2App.py".

References

Bekaert, D. P. S., R. J. Walters, T. J. Wright, A. J. Hooper, and D. J. Parker (2015), Statistical comparison of InSAR tropospheric correction techniques, Remote Sensing of Environment, 170, 40–47, doi:10.1016/j.rse.2015.08.035.

Berardino, P., G. Fornaro, R. Lanari, and E. Sansosti (2002), A new algorithm for surface deformation monitoring based on small baseline differential SAR interferograms, IEEE Trans. Geosci. Remote Sensing, 40(11), 2375–2383, doi:10.1109/TGRS.2002.803792.

Blewitt, G., W. Hammond, and C. Kreemer (n.d.), Harnessing the GPS Data Explosion for Interdisciplinary Science, Eos, 99, doi:10.1029/2018EO104623

Gomba, G., F. Rodriguez Gonzalez, and F. De Zan (2016), Ionospheric Phase Screen Compensation for the Sentinel-1 TOPS and ALOS-2 ScanSAR Modes, IEEE Trans. Geosci. Remote Sensing, 55(1), 223–235, doi:10.1109/TGRS.2016.2604461.

Liang, C., & Fielding, E. J. (2017a). Interferometry With ALOS-2 Full-Aperture ScanSAR Data. IEEE Transactions on Geoscience and Remote Sensing, 55(5), doi:10.1109/TGRS.2017.2653190

Liang, C., and E. J. Fielding (2017b), Measuring Azimuth Deformation With L-Band ALOS-2 ScanSAR Interferometry, IEEE Transactions on Geoscience and Remote Sensing, 55(5), 2725-2738, doi:10.1109/TGRS.2017.2653186.

Liang, C., Z. Liu, E. J. Fielding, and R. Bürgmann (2018), InSAR Time Series Analysis of L-Band Wide-Swath SAR Data Acquired by ALOS-2, IEEE Trans. Geosci. Remote Sensing, 56(8), 4492–4506, doi:10.1109/TGRS.2018.2821150.

Jolivet, R., R. Grandin, C. Lasserre, M. P. Doin, and G. Peltzer (2011), Systematic InSAR tropospheric phase delay corrections from global meteorological reanalysis data, Geophysical Research Letters, 38(17), L17311, doi:10.1029/2011GL048757.

Rosen, P. A., E. Gurrola, G. F. Sacco, and H. Zebker (2012), The InSAR Scientific Computing Environment, paper presented at 9th European Conference on Synthetic Aperture Radar, Nuremberg, Germany, 23-26 April.

Schmidt, D. A., and R. Bürgmann (2003), Time-dependent land uplift and subsidence in the Santa Clara valley, California, from a large interferometric synthetic aperture radar data set, J. Geophys. Res., 108(B9), 1985, doi:10.1029/2002JB002267.

Tong, X., D. Sandwell, and B. Smith-Konter (2013), High-resolution interseismic velocity data along the San Andreas fault from GPS and InSAR, J .Geophys. Res., 118, doi:10.1029/2012JB009442.

Tymofyeyeva, E., and Y. Fialko (2015), Mitigation of atmospheric phase delays in InSAR data, with application to the eastern California shear zone, J. Geophys. Res. Solid Earth, 120(8), 5952–5963, doi:10.1002/2015JB011886.